Int. J. Electrochem. Sci., 9 **(2014)** 6191 - 6200

International Journal of
ELECTROCHEMICAL
SCIENCE
www.electrochemsci.org

Tunable Photonic Crystals Based on Electrochemically Etched Porous Silicon

Niel Gabriel E. Saplagio[*], *Arvin I. Mabilangan, Maria Angela B. Faustino, Lorenzo P. Lopez Jr., Armando S. Somintac and Arnel A. Salvador*

Condensed Matter Physics Laboratory, National Institute of Physics, University of the Philippines, Diliman, Quezon City, Philippines
[*]E-mail: nsaplagio@nip.upd.edu.ph

Received: 20 April 2014 / *Accepted:* 19 June 2014 / *Published:* 25 August 2014

In this paper, porous silicon photonic crystals were simulated and fabricated as distributed Bragg reflectors (DBRs), graded DBRs and Fabry-Perot (FP) filters. The transfer matrix method (TMM) was used to model the propagation of light in the photonic crystal. The porous silicon photonic crystals were fabricated by electrochemically etching p-type (100) silicon in 12% hydrofluoric acid solution. Applied currents of 20mA and 120mA were used to produce the varying refractive indices of the layers. Distributed Bragg reflectors were tuned to have their central wavelength at 650nm, 700nm, and 800nm while the FP filter optical cavity was tuned to 650nm. Results show the effective formation of uniform and graded DBR with maximum gradation of 300nm. Simulation of DBR and FP reflectivity yielded a maximum of 2.51% and 0.37% deviation from the simulated values. Results show that the experimental data was in good agreement with the simulated reflectivity at the different central wavelengths. The paper has shown the ease and versatility in the fabrication of porous silicon as photonic crystals.

Keywords: Porous silicon, Electrochemical etching, Transfer Matrix Method, Distributed Bragg Reflector, Fabry-Perot filter, Photonic crystal.

1. INTRODUCTION

Porous silicon is a composite material composed of crystalline silicon and air. It is made by electrochemically etching the surface of silicon in a hydrofluoric acid solution. It trumps other fabrication techniques due to the abundance of silicon and the simplicity of fabrication. Due to its variable porosity, porous silicon was found to have optical applications in solar cells [1]; light emitting diodes [2]; interferometry sensors [3]; vertical cavity surface emitting lasers [4]; Rugate [5] and Fabry-

Perot filters [6]; and chemical and gas sensors [7]. One of the most useful and yet versatile products of porous silicon are photonic crystals.

Photonic crystals act as waveguides for light. In one dimension, these are called DBRs. They are multilayered structures made up of layers with varying thickness and index of refraction. These layers, when tuned properly, can reflect light at selected regions of wavelengths. Since the fabrication parameters of porous silicon dictate its film thickness and porosity, its refractive index per layer can be chosen or tuned. Bragg reflectors are used widely in optics as optical filters, detectors, or reflectors in solar cells and lasers. DBRs can also be modified to absorb a much narrower set of wavelengths by adding a spacer layer or an optical cavity between two DBR stacks. Such a device is called a Fabry-Perot filter and is used similarly for detection and absorption. These photonic crystals can be fabricated to be uniform or graded depending on the application with the latter having colorimetric applications through integrated devices such as photometers [8].

The most common technique in characterizing porous silicon is by obtaining its reflectivity spectrum [9]. Through the spectral reflectivity of the porous silicon, its refractive index can be calculated. After doing so, multilayers can now be fabricated using these parameters. The reflectivity of porous silicon was simulated using the TMM. In this paper, we present the reflectivity simulation of DBRs and FP based on the TMM and the electrochemical formation of uniform and graded distributed Bragg reflectors, as well as Fabry-Perot filters.

2. EXPERIMENTAL DETAILS

Prior to the experiment, p-type silicon (100) wafers with resistivity of 0.01–10.0 Ω•cm, were subjected to standard degreasing procedures. These samples were then subjected to varying anodic currents and etch times to be able to find the relation between the anodization parameters (etch time and current) with the porosity and thickness of the porous silicon layers. The calibration details of which can be found in a paper published in this journal: [10]. The etchant used was composed of 12% HF solution mixed with equal parts of absolute ethanol. The current source used in the experiment was a Tektronix programmable power supply. A silver plate was used as the counter electrode of the setup. The samples were dried by rinsing it with ethanol and allowing it to dry in ambient air. Afterwards, cross section scanning electron microscope measurements were done to verify the thickness of each calibration layer, while reflectance measurement was done to obtain the effective refractive index of the samples.

The propagation of light through porous silicon and its consequent reflection on the sample was simulated by using the TMM. Since light is an electromagnetic wave, one can use vectors in order to analyze its propagation through a medium. The TMM offers a simple yet approximate prediction of the behavior of light in any kind of medium. Using the simulation, three different DBRs were tuned to 650nm, 700nm, and 800nm peak wavelengths. The etching parameters are summarized in Table 1. The DBRs were fabricated by changing the applied current with respect to time. Each DBR were designed to have 5 stacking pairs.

Table 1. Parameters for DBR centered at 650nm, 700nm, and 800nm.

Color	Layer	Anodic current (mA)	Etch time (s)
Red (650 nm)	n_1	20	24
	n_2	120	12
Near Infrared (700 nm)	n_1	20	34
	n_2	120	16
Infrared (800 nm)	n_1	20	51
	n_2	120	21

Normal incidence reflectance spectroscopy was done to obtain the reflectance of all the samples from 400nm to 1100nm. A 100W tungsten halogen lamp was used as the light source of a SPEX 100M single grating monochromator. A series of lenses was used to focus the reflected light from the sample into a silicon photodiode. The photodiode was then connected to an SR-380 lock-in amplifier for standard lock-in signal acquisition. All samples were normalized to a reference aluminum mirror to obtain the reflectance of the sample. Figure 1 shows the schematic of the setup used for optical reflectivity.

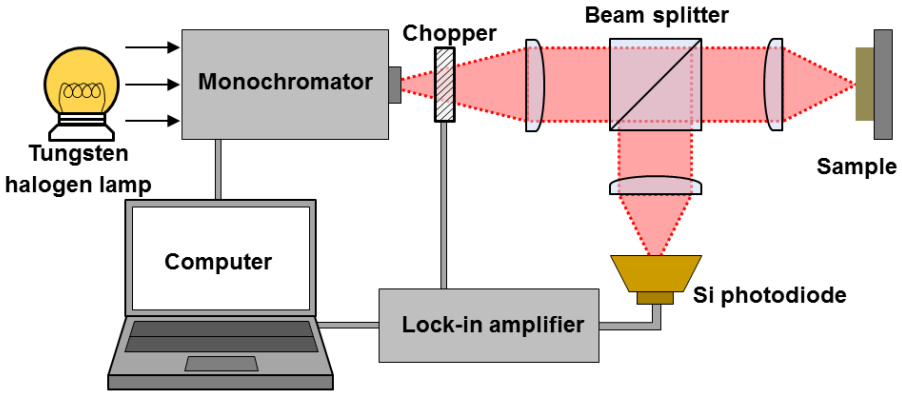

Figure 1. Schematic diagram of optical reflectivity

Table 2. Etching parameters for graded DBR fabrication

DBR Color	Layer	Anodic current (mA)	Etch time (s)
Yellow (570-590 nm)	n_1	20	39
	n_2	120	17
Green (495-570 nm)	n_1	20	34
	n_2	120	15
Red (620-750 nm)	n_1	20	45
	n_2	120	20

Graded DBR samples were also etched with similar parameters but at a 20º anode angle from the usual parallel. This was done to maximize the variation in porosity produced by the difference in

the potential at the top and bottom of the sample [11]. The etching parameters are found in Table 2. The graded DBRs were fabricated to have 5 stacking pairs.

For the FP samples, a spacer layer was added in between two DBR with a 5 stacking pairs structure in order to form an optical cavity in the reflectivity spectrum [12]. This would vary the reflectance spectrum of a typical DBR by incorporating a narrow bandpass in the peak reflectance region of the DBR. The etching parameters of the FP filter are shown in Table 3.

Table 3. Parameters for Fabry-Perot filter fabrication

Layer	Anodic current (mA)	Etch time (s)
n_1	20	28
n_2	120	14
spacer	40	28

3. RESULTS AND DISCUSSION

3.1. Single layer Porous Silicon

In order to tune the Distributed Bragg reflectors, single layer porous silicon were first fabricated. Shown in Figure 2 are the top and cross section SEM images of the porous silicon single layers. These samples were also characterized through reflectance spectroscopy. Shown in Figure 3a are the reflectivity of two different layers of porous silicon etched at 20mA and 120mA respectively. From the thickness and reflectivity, the index of refraction of the respective porous silicon single layers was obtained. This was done by fitting the indices of refraction based on consecutive reflectivity peaks, with a Sellmeier fit as shown in Equation 1. The Sellmeier fit of the refractive index is shown in Figure 3b. The 20mA current was observed to have a higher index of refraction compared to 120mA as seen in the figure. This difference was due to the difference in the porosity of porous silicon with higher current producing higher porosity and consequently lower refractive index [10, 13]. This variation of refractive index with changing anodization current was then used to design and simulate the various porous silicon multilayers.

$$n^2 = A + \frac{Bx^2}{x^2 - C^2} + \frac{Dx^2}{x^2 - E^2} \quad (1)$$

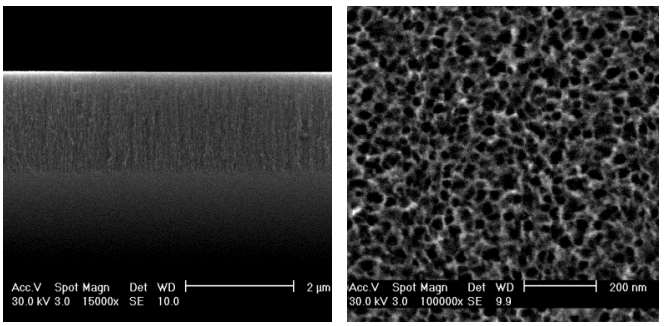

Figure 2. Cross section and top view SEM images of single layer porous silicon.

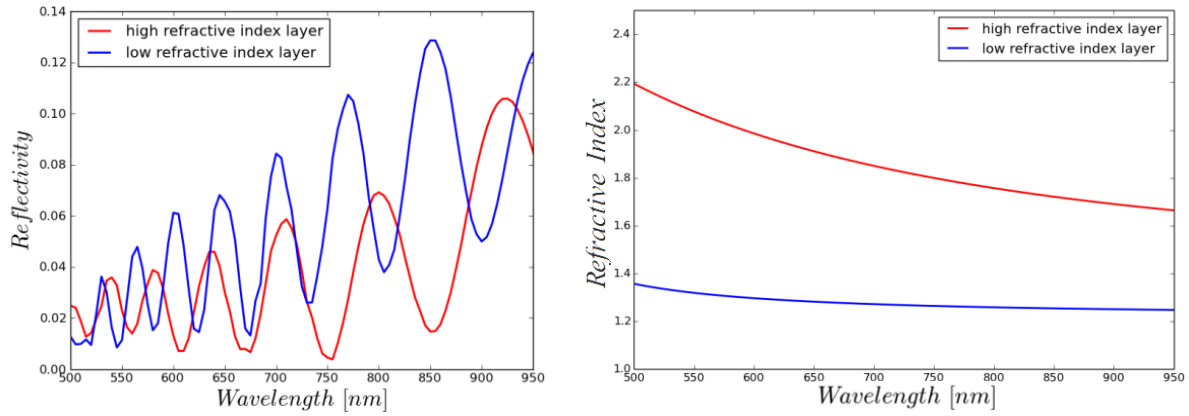

(a) (b)

Figure 3. The (a) reflectivity of porous silicon with different refractive indices and (b) the calculated Sellmeier refractive index.

3.2. Design and Simulation of DBR

The ability of a DBR to reflect a certain range of wavelength comes from its unique structure. Since it is a periodic multilayer thin film, the reflection of light at each interface also varies periodically. A quarter wave stack is formed because the product of the index of refraction and thickness of each layer is equal to one fourth of the desired central wavelength as shown in Equation 2.

$$n_i d_i = \frac{\lambda}{4} \tag{2}$$

Constructive interference occurs at these conditions and the light is highly reflected at the desired wavelength. This is exhibited by a peak in the reflectivity spectrum of the sample. The TMM is a technique that can be used to investigate the propagation of light in different media. It is a mathematical technique used to obtain the state of electromagnetic wave propagating in a multilayered structure [13]. This technique was also implemented on simulation studies for reflectivity spectrum of DBRs [14-15]. The general formula for this is given by Equation 3.

$$\begin{bmatrix} E_j^+ e^{ik_j z} \\ E_j^- e^{-ik_j z} \end{bmatrix} = \mathbf{S}_{j+1} \begin{bmatrix} E_{j+1}^+ e^{ik_{j+1} z} \\ E_{j+1}^- e^{-ik_{j+1} z} \end{bmatrix} \tag{3}$$

where

$$\mathbf{S}_j = \frac{1}{t_{j,j+1}} \begin{bmatrix} e^{i\delta_j} & r_{j,j+1} e^{i\delta_j} \\ r_{j,j+1} e^{-i\delta_j} & e^{-i\delta_j} \end{bmatrix} \tag{4}$$

The variable S is called the transfer matrix for each media $j = 1, 2, 3\ldots N$ where N is the number of interfaces between the different media. The phase of the wave is given by $\delta_j = k_j d_j$, where k is the wavenumber and d is the thickness of the media. Included in the transfer matrix are the reflection and transmission coefficients given by equations 5 and 6.

$$r_{j,j+1} = \frac{n_j - n_{j+1}}{n_j + n_{j+1}} e^{2ik_j z} \tag{5}$$

$$t_{j,j+1} = \frac{2n_j}{n_j + n_{j+1}} e^{i(k_j + k_{j+1})z} \quad (6)$$

From these equations, the generalized reflection intensity is given by Equation 7.

$$R = \left| \frac{\mathbf{S}_{21}}{\mathbf{S}_{11}} \right|^2 \quad (7)$$

These equations were used to simulate the reflectivity of the.

3.3. Uniformity of the DBRs

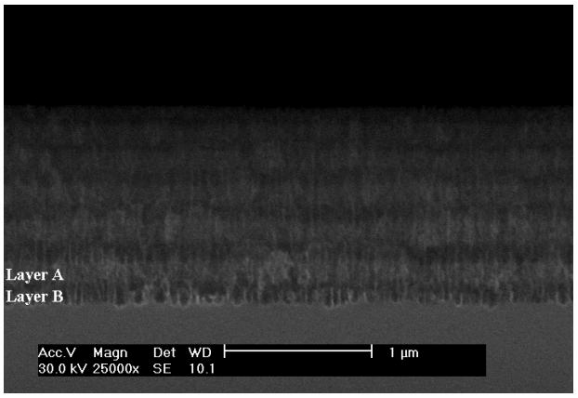

Figure 4. Cross section SEM image of a porous silicon DBR.

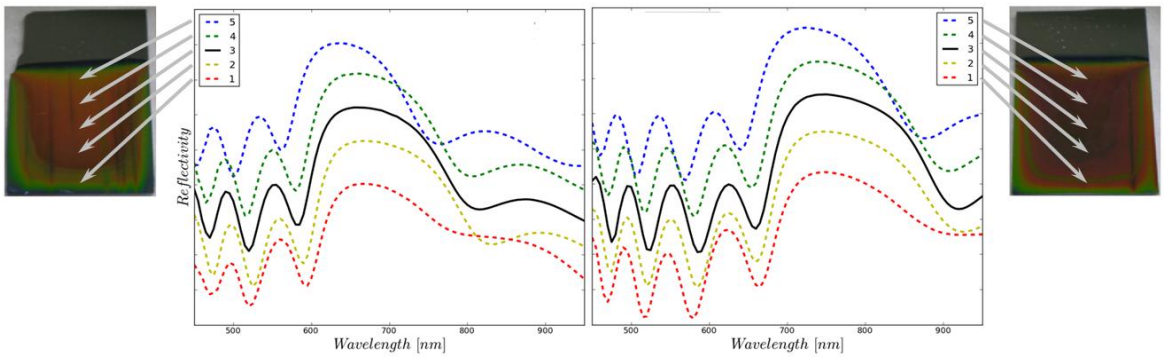

(a) (b)

Figure 5. Position dependent reflectivity of DBR centered on (a) 700nm and (b) 800nm with sample inset.

Figure 4 shows the cross section SEM image of a DBR that was tuned to have a central wavelength at 650nm. It can be seen that the thickness of each layer periodically varies together with its porosity and consequently its refractive index in the in-plane direction. In Figure 5 the position dependent reflectivity of the DBR fabricated to have central wavelengths at 700nm and 800nm is shown. The reflectivity of the multilayers minimally varies as indicated by the closeness of the position dependent scans. The bandwidth shift was observed to be present only at the top of the sample

which is attributed to the existing potential difference in the air-solution interface during anodization. Successive positions show that uniform bandwidth and peak positions were obtained throughout the sample. These plots show that uniform porous silicon DBRs can be fabricated easily with this configuration and is in agreement with [16]. The next part compares the simulated and experimental reflectivity obtained in the experiment.

3.4. DBR Reflectivity Simulation

Shown in Figure 6 are the simulated and experimental reflectivity plots of the DBR tuned at center wavelengths of 650nm, 700nm, and 800nm. From the plot, it can be observed that the peak reflectivity coincides with the simulated reflectivity. However the central wavelengths for all the DBR were shifted to shorter wavelengths. This could have been due to the averaging error from computing the index of refraction from the extremum values of the reflectivity spectrum. The values for the simulated and experimental central wavelengths are summarized in Table 4. The %deviation of each DBR is also included. The maximum deviation obtained was 2.50% corresponding to the DBR tuned at 800nm.

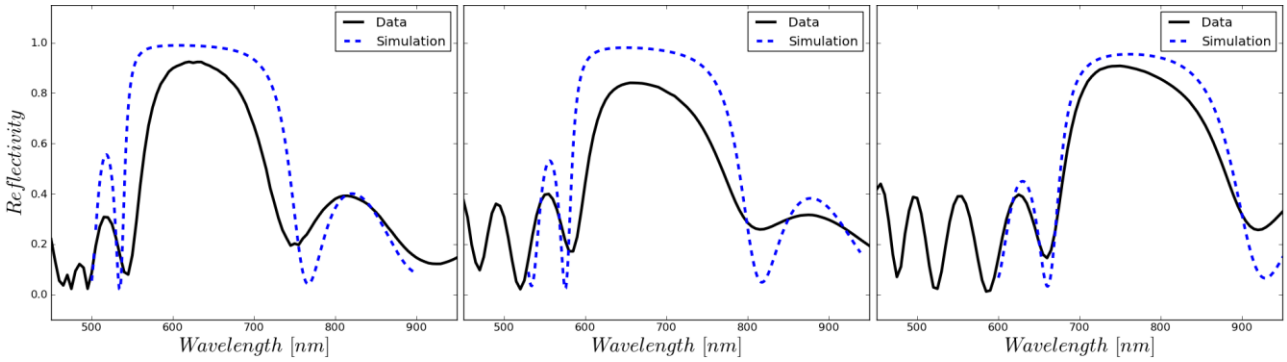

Figure 6. Simulated and Experimental data of DBR centered at (a) 650nm, (b) 700nm, and (c) 800nm.

Table 4. Simulated and experimental central wavelength along with their corresponding % deviation.

Simulated (nm)	Experimental (nm)	% Deviation
800	780	2.50
700	685	2.14
650	635	2.31

3.5. Graded Distributed Bragg Reflectors

The reflectivity spectra of the graded DBRs are shown in Figure 7 along with their sample images. Optical materials that have graded properties such as these are helpful in fabrication of colorimetric devices such as photometers as mentioned above. It is noticeable that compared to the

uniform DBR produced previously, these samples exhibit controlled variation of central wavelength position as observed from the shifting central wavelength compared to that of grin lenses produced in a single cell setup[17]. These samples were found to have as much as 300nm shift in their central wavelength as shown by the colorful sample image inlayed in the plots. This shift in reflectance was also observed from other methods of producing graded multilayered structures [18-19].

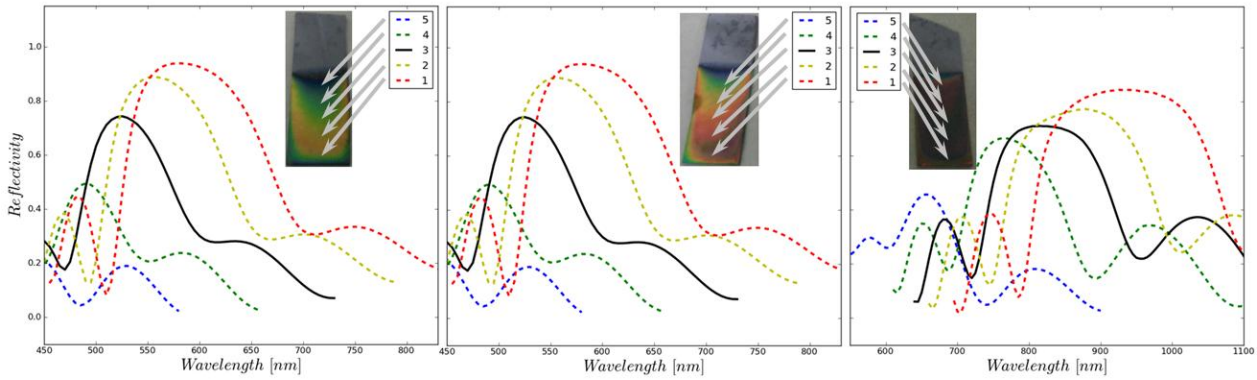

(a) (b) (c)

Figure 7. Position dependent reflectivity for graded porous silicon DBR in the (a) green, (b) yellow, and (c) red range of wavelengths.

3.6. Fabry-Perot Filter

The fabricated FP filters were created by introducing a spacer layer in between the two successive DBR stacks. This structure can be used to reflect a wide range of wavelength leaving but a small region transmitted.

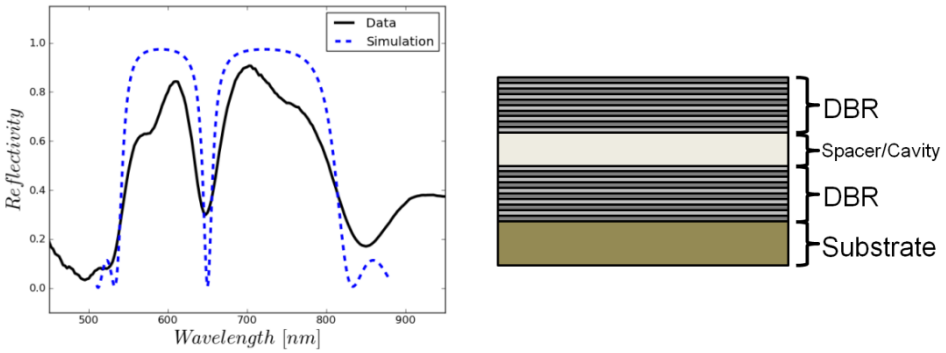

(a) (b)

Figure 8. (a) Simulated and Experimental reflectivity of a Fabry-Perot filter with an optical cavity centered at 650nm. (b) Schematic diagram of the Fabry-Perot filter.

This mechanism is helpful in optics as light filters or partial reflectors. Shown in Figure 8 below is the manifestation layer as a cavity in the DBR reflectivity along with the structure of the FP

filter. This cavity acts as a region where certain wavelengths are absorbed or transmitted in porous silicon as shown by the dip in peak wavelength of the DBR. The result was found to agree with other papers such as [12]. The simulated and experimental peak reflectivity as well as its % deviation is shown in Table 5. The % deviation obtain from the FP filter was found to be 0.37% showing very good agreement with the simulated value. However, the decrease and loss in the intensity in Fabry Perot is due to identical losses in each of the layers [20]

Table 5. Simulated and Experimental cavity position of the FP filter centered at 650nm.

Simulated (nm)	Experimental (nm)	% Deviation
650	647.5	0.37

4. CONCLUSION

Porous silicon photonic crystals were successfully electrochemically etched from crystalline silicon. The fabricated DBRs were found to have good uniformity with varying position in the sample. The experimentally obtained reflectivity deviated from the simulated reflectivity with a maximum value of 2.51% for the three DBRs fabricated. Furthermore, graded DBRs were also shown to have maximum gradation of 300nm while the fabricated FP filter was shown to have only a 0.37% deviation from the simulated reflectivity. The experiment has shown the ease and versatility in the fabrication of porous silicon photonic crystals as uniform and graded DBRs and Fabry-Perot filter structures through anodization.

ACKNOWLEDGEMENT
This work was funded in part by the National Research Council of the Philippines and the Department of Science and Technology (DOST)-Philippine Council for Industry, Energy and Emerging Technology Research and Development.

References

1. P. Vitanov, E. Goranova, V. Stavrov, P. Ivanov, PK Singh. Solar *Energy Materials and* Solar Cells, 93 (2009) 297.
2. Barillaro G, Pieri F, Mastromatteo U. *Optical Materials*. 17(1) (2001) 91-94
3. HJ Kim, YY Kim, KW Lee, SH Park. *Sensors and Actuators B: Chemical*, 155(2) (2011) 673-678.
4. M. Abid, T. Moudakir, Z. Djebbour, G. Orsal, S. Gautier, A Naciri, A. Migan-Dubois, A. Ougazzaden. *Journal of Crystal Growth*, 315 (2011) 283-287.
5. S. Um, J. Yang, TE Choi, H. Cho, S. Jin, H. Sohn. *Microelectronic Engineering*, 89 (2012) 100-103.
6. J. Volk, J. Balázs, AL Tóth, I. Bársony. *Sensors and Actuators B: Chemical*, 100 (2004) 163-167.
7. S. Ozdemir, JL Gole. Sensors *and Actuators B: Chemical.* 151 (2010) 274-280.
8. D. Hunkel, M. Marso, R. Butz, R. Arens-Fischer, H. Lüth. *Materials Science and Engineering: B.* 69 (2000) 100-103.
9. N. Samuoliene, E. Šatkovskis. *Nonlinear Analysis: Modelling and Control* 10(1) (2005) 83–91

10. A. Mabilangan, N Saplagio, E. Anguluan, N. Cabello, R. Gonzales, A. Somintac, A. Salvador. *Science Diliman.* 25 (2013) 15-28
11. R.E. Marotti, A. Rondoni, E. Quagliata, E.A. Dalchiele. *Physica Status Solidi B*. 220(1) (2000) 319-324
12. TC Do, H Bui, TV Nguyen, TA Nguyen, TH Nguyen, VH Pham. *Adv. Nat. Sci.: Nanosci. Nanotechnol.* 2 (2011)
13. J. Torres, F. Castillejo, J.E. Alfonso, *Brazilian Journal of Physics*, 36 (2006) 1021-1024
14. B.E. Sernelius, "Chapter 3 – Simulation programs for the analysis of multilayered media," *Lectures of B.E. Sernelius*, p.13:1-13:11
15. NH Maniya, SR Patel, ZVP Murthy. *International Journal of Light and Electron Optics*. 125 (2014) 828–831.
16. A. Palavicini, C. Wang. *Optics and Photonics Journal*, 3 (2013) 20-25
17. O. Fellahi, T. Hadjersi, Y. Ouadah. *Physics Procedia*. 2(3) (2009) 759–764
18. S. Ilyas, M. Gal. *International Journal of Nanotechnology*, 5(2-3) (2008) 163-169
19. K. Hwang, S. Kim, Y. Park, H. Jeon, J. Jeong. *Journal of Applied Optics*. 47(10) (2008) 1628-1631.
20. D Hunkel, M Marso, R Butz, R Arens-Fischer, H Lüth. *Materials Science and Engineering: B* 69 (2000) 100-103.
21. U.C. Hasar, I. Y. Ozbek, E. A. Oral, T. Karacali, and H. Efeoglu. *Optics Express*, 20(20) (2012) 22208-22223